TOF-SIMS Evidence of Intercalated Molecular Gases and Diffusion-Limited Reaction Kinetics in an α Particle-Irradiated PTFE Matrix

Gregory L. Fisher,*,†,‖ Christopher Szakal,‡ Christopher J. Wetteland,§ and Nicholas Winograd‡

Nuclear Materials Technology (NMT-16), Los Alamos National Laboratory, P.O. Box 1663, Los Alamos, New Mexico 87545, Department of Chemistry, The Pennsylvania State University, 104 Chemistry Building, University Park, Pennsylvania 16802, and Materials Science and Technology (MST-8), Los Alamos National Laboratory, P.O. Box 1663, Los Alamos, New Mexico 87545

Received: September 22, 2005; In Final Form: November 28, 2005

The chemical evolution of poly(tetrafluoroethylene) (PTFE) that is brought about by increasing levels of irradiation with α particles is accompanied by the emergence and proliferation of functionalized moieties. Families of reaction products specifically identified in the α-irradiated polymer matrix include hydride-, hydroxide-, and oxide-functionalized fluorocarbons. The data also indicate the emergence of hydrogen peroxide (H_2O_2) and hydrazine (N_2H_4), but no distinct evidence suggesting the formation of perfluorinated amines, amides, or cyanogens is found. In this article we substantiate the speciation of emergent species and reveal evidence of intercalated molecular gases with which α particle-generated radicals may react to form the observed products. Furthermore, we present evidence to suggest that the kinetics of α particle-induced reaction is limited by the diffusion of radicals within the polymer matrix. That is to say, chemical additives in the polymer matrix are shown to be scavengers of H•, O•, and F• radicals and limit the rates of reaction that produce functionalized fluorocarbon moieties. Above a threshold dose of α particles, the concentration of radicals exceeds that of the scavenger species, and free radical diffusion commences as evidenced by a sudden increase in the yield of reaction products. Samples of PTFE were irradiated to α doses in the range of 10^7 to 5×10^{10} rad with 5.5 MeV $^4He^{2+}$ ions from a tandem accelerator. Residual gas analysis (RGA) was utilized to monitor the liberation of molecular gases from PTFE during α particle irradiation of samples in vacuum. Static time-of-flight SIMS (TOF-SIMS), equipped with a 20 keV C_{60}^+ source, was employed to probe chemical changes as a function of α particle irradiation. Chemical images and high-resolution mass spectra were collected in both the positive and negative polarities.

1. Introduction

The chemistry of radiation-modified poly(tetrafluoroethylene) (PTFE) is complex and seemingly counterintuitive, as has been demonstrated in the literature by several groups.[1−5] For instance, Lunkwitz and co-workers irradiated PTFE with MeV β particles in the presence of air, in N_2 gas at atmospheric pressure, and in vacuum, and probed the samples using infrared spectroscopy (IRS).[1,2] They reported varying degrees of cross-linking and branching, unsaturation, and incorporation of oxygen in the form of acyl fluoride and carboxylic acid groups. No nitrogen-functionalized species were reported. Additional studies performed in the presence of inert (N_2, Ar) and reactive (O_2) atmospheres indicate that β particle irradiation of PTFE in a reactive atmosphere results in a higher rate of polymer decomposition accompanied by the formation of oxyl and peroxyl species.[3] Still, with regard to specimens irradiated in the presence of N_2, no mention was made concerning the emergence of nitrogen-functionalized species. Wilson et al. investigated the plasma treatment of PTFE using Ar, NH_3, N_2, and O_2 gases.[4] All plasma treatments resulted in defluorination, unsaturation, and oxygen functionalization. Nitrogen incorporation was found to occur only in the NH_3- and N_2-treated specimens which were shown to contain amine, amide, and cyano compounds by X-ray photoelectron spectroscopy (XPS); however, no secondary ion mass spectrometry (SIMS) data were available to support these structures. Most notably observed in the SIMS spectra were ingrowth of hydrogen- and oxygen-functionalized moieties. Interestingly, the Ar-treated specimens were found to have the highest ratios of hydrogen and oxygen to carbon. Ultraviolet (UV) irradiation of PTFE in vacuum and in atmospheres of NH_3 and N_2H_4 was performed by Heitz et al.[5] As determined by XPS and SIMS, all specimens were shown to have incorporated oxygen, while only those treated in NH_3 or N_2H_4 atmospheres were shown to have incorporated nitrogen. The preceding experiments all involve irradiation of the samples with a low linear energy transfer (LET) source. A high LET source, such as α particle radiation, deposits more energy over a shorter distance thereby creating more reaction centers per unit volume.[6] As a result, it is expected that α particle irradiation of PTFE would result in a greater diversity of reaction products that would necessitate the use of a high-resolution structural probe, such as time-of-flight SIMS (TOF-SIMS), to characterize.

We have recently reported our observations regarding the effects of MeV α particle radiation on PTFE.[7,8] TOF-SIMS was used to probe the effects of 5.5 MeV α particles on the polymer

* Corresponding author. E-mail: glfisher@lanl.gov.
† Nuclear Materials Technology, Los Alamos National Laboratory.
‡ The Pennsylvania State University.
§ Materials Science and Technology, Los Alamos National Laboratory.
‖ Current address (as of Feb 2006): Physical Electronics USA, 18725 Lake Drive East, Chanhassen, MN 55317.

10.1021/jp055402d CCC: $33.50
Published on Web 01/11/2006

matrix in the dose range of 10^7 to 10^{11} rad. To summarize, we observed cross-linking at α doses of $<10^{10}$ rad accompanied by increased fragmentation and unsaturation at α doses $>10^9$ rad. At α doses $>10^{10}$ rad, extreme structural degradation of the polymer was manifested by the proliferation of low-mass fluorocarbons. The polymer degradation was accompanied by fluorocarbon functionalization that was observed at the lowest dose of α particles and appeared to escalate with increasing α particle irradiation. In particular, our data indicated that α particle-induced reaction was accelerated at α doses $\geq 10^9$ rad. Groups of reaction products that have been identified include olefins and paraffins of oxyl- and peroxyl-functionalized fluorocarbons, as well as hydrocarbons. The origin of the oxyl and peroxyl moieties has been explained in terms of the decomposition of perfluorinated polyether residues and reaction of α particle-generated fluorocarbon radicals with molecular oxygen, atomic oxygen, and O• radicals.[8] The formation of hydrocarbons currently lacks complete resolution. Reasonable mechanisms include reaction of α particle-generated radicals from the defluorinated polymer matrix with hydrogen radicals or molecular hydrogen and reaction of radiolized hydrocarbon additives in the polymer matrix with fluorine radicals. Either mechanism would be substantiated, at least in part, by the appearance of fragments having the general composition of $C_xH_yF_z^{\pm}$ in the mass spectra.

In this article we present supplementary evidence in support of the reaction of primary and secondary fluorocarbon radicals to form hydro, hydroxyl, oxyl, and peroxyl moieties. Substantiation of data discussed in a previous article[8] is also provided regarding the occurrence of oxygen-bearing molecular gases, with which α particle-generated radicals react to produce functionalized fluorocarbons, in the polymer matrix. Furthermore, the signals of reaction products bear evidence of a mechanism wherein the kinetics are diffusion-limited. In other words, the reaction rates are limited by the ability of α particle-generated radicals to diffuse within the polymer matrix. Analysis of the data leads to the conclusion that radiolytic decomposition products of isoparaffins, chemical additives used in the manufacture of PTFE,[9,10] behave as scavengers of H•, O•, and F• radicals. At a threshold dose of α particles, the rate of reaction is observed to increase from which we infer that the concentration of radicals exceeds that of the scavenger species. These results further imply that surface reactions, i.e., between radicals and gases coincident at the sample surface, provide only a minor contribution to the observed ion signals.

TOF-SIMS was used to characterize the cumulative effects of MeV α particles on the PTFE matrix as well as the functionalized reaction products. Residual gas analysis (RGA) was utilized to monitor the liberation of molecular gases from the PTFE matrix during α particle irradiation of samples in vacuum. These results corroborate previous conclusions and provide a rational explanation for the functionalization observed to occur in perfluorinated polymers irradiated by a number of methods in ostensibly inert conditions (e.g., vacuum, Ar, or N_2 atmospheres).

2. Experimental Section

2.1. Sample Preparation. Neat PTFE in 2 mm thick sheets was purchased from Goodfellow (Berwyn, PA, P/N FP303100) for use in these experiments. Nitrile gloves were donned prior to handling samples, and all manipulation was accomplished with methanol-cleaned and nitrogen-dried tools. Specimens were cut from the sheet stock, mounted in the sample holder, and introduced into the vacuum vessel for irradiation. The irradiation chamber is attached to the tandem accelerator beam line but separated from it by several skimmed differential pumping stations. The irradiation chamber vacuum system consists of a 510 L/s turbopump backed by a mechanical pump. A pressure of $<1 \times 10^{-6}$ torr was achieved before irradiation of each sample. As determined by RGA, the background was comprised of common vacuum contaminants including H_2, H_2O, CO/N_2, O_2, and CO_2 at partial pressures commensurate with the total pressure.

2.2. α Irradiation. The irradiation of PTFE by α particles was accomplished using 5.5 MeV $^4He^{2+}$ ions generated in a tandem accelerator beam line. The samples were exposed to a ~0.3 cm diameter continuous (DC) beam that was scanned over the exposed portion of the sample. The samples were nominally maintained at room temperature while irradiated to nominal α doses of 10^7, 10^8, 10^9, 10^{10}, and 5×10^{10} rad. For comparison, 1 rad is equivalent to 0.01 gray (Gy) and 100 erg/g. Samples prepared for TOF-SIMS analysis were irradiated at beam currents of 5 nA for doses $\leq 10^8$ rad, 15 nA at a dose of 10^9 rad, and 25 nA for doses $\geq 10^{10}$ rad. Samples used during RGA were irradiated at a beam current of 40 nA. Irradiation was performed in continuous fashion for each nominal dose. The relative error in the cumulative dose measurements is ±10%. Following irradiation, the samples were pulled from the irradiation chamber, loaded into wafer holders, and stored in ambient conditions for subsequent analysis.

2.3. Gas Analysis. Evolution of H_2O, CO/N_2, O_2, and CO_2 was monitored during α particle irradiation of the samples using a quadrupole-based residual gas analyzer (Stanford Research Systems, Sunnyvale, CA, P/N RGA200). The pressure versus time scans were performed under the conditions of a 1 mA emission current, a 70 V accelerating voltage, a gain of approximately 1000, and a 1 s sampling period. The ionizer of the RGA was positioned approximately 7 in. from the specimen during analysis and was not mounted within line-of-sight of the samples. The thoriated iridium filaments were thoroughly degassed prior to experimental data acquisition.

2.4. TOF-SIMS Analysis. TOF-SIMS analysis was performed using a custom instrument, described in detail elsewhere,[11] approximately 2 weeks following irradiation. The system is equipped with a sorption-pumped chamber for fast sample introduction to a turbopumped antechamber and an ion-pumped analysis chamber with a base pressure of $\sim 1 \times 10^{-9}$ torr. Nitrile gloves were donned prior to handling samples, and all manipulation was accomplished with methanol-cleaned and air-dried tools. The PTFE samples were mounted on a sample holder and were loaded into the vacuum system which was pumped down to $<1 \times 10^{-6}$ torr before transfer of the samples to the analytical chamber. Secondary ions for mass spectral and chemical image acquisition were generated using a 20 keV C_{60}^+ ion source focused to a diameter of ≤ 30 μm at the sample.[12] During data acquisition the primary ion beam conditions were a pulse width of 50 ns at 3 kHz and a dc current of 0.54 nA. The raster area was 200×200 μm^2 during spectrum acquisition and 400×400 μm^2 during imaging. Mass spectra were acquired with the raster area completely within or outside the irradiated portion of the sample, while images were always collected at the boundary of the irradiation zone. In the course of spectrum acquisition, approximately 2.7×10^{11} C_{60}^+/cm^2 impinged the surface of the analytical area, an order of magnitude below the static limit.[13] The total ion dose during imaging was one-fourth the total ion dose used for spectrum acquisition. In the positive polarity, analyses were performed with a nominal mass resolution ($m/\Delta m$) of ~2500 in the mass-to-charge (m/z) region below

100 *m/z*. The mass resolution in the negative polarity was <500 in the same mass-to-charge range. No charge compensation was required during spectrum or image acquisition.

3. Results

The TOF-SIMS spectra were collected in the range of 4−1800 *m/z* in both the positive and negative polarities. In general, the total counts of the negative ion spectra are $<^1/_{16}$ the total counts of the positive ion spectra. A total of three neat PTFE samples were analyzed. Each sample included the α radiation doses described in section 2.2. Within each zone at least two different areas were analyzed. A single image was acquired at the boundary of each irradiation zone of each sample.

For mass spectral features related to the polymer matrix, relative peak intensities were generally reproducible to within ±20% from sample to sample. Where quantitative correlations are made, measurements from all samples were used to determine the mean and standard deviation of the measurement. Data values greater than one standard deviation (1σ) from the estimated mean were excluded from the data set, and the mean was calculated using a minimum of three data points for each measurement. Outliers are straightforwardly attributed to sample-to-sample variation and morphological roughness at α doses $\geq 10^{10}$ rad since sample charging was not observed to be a problem during analysis.

The fingerprint peaks of unirradiated PTFE are found in the positive ion spectra below 200 *m/z* with a few additional peaks of the characteristic form $[C_nF_{2n-1}]^+$ extending out to 400 *m/z*.[14,15] In general, the relative intensities of the fingerprint peaks provide a useful indication that the samples were prepared and handled without significant incorporation of impurities. Characteristic fragment ions and their nominal mass-to-charge ratios are CF^+ (31 *m/z*), CF_2^+ (50 *m/z*), CF_3^+ (69 *m/z*), $C_3F_3^+$ (93 *m/z*), $C_2F_4^+$ (100 *m/z*), $C_2F_5^+$ (119 *m/z*), and $C_3F_5^+$ (131 *m/z*). In the negative ion spectrum, the characteristic peaks of PTFE include CF^- (31 *m/z*), CF_3^- (69 *m/z*), $C_3F_3^-$ (93 *m/z*), and $C_2F_5^-$ (119 *m/z*). Silicone residues were observed to be present as indicated by the positive ions SiH^+ (29 *m/z*), CH_3Si^+ (43 *m/z*), $SiOH^+$ (45 *m/z*), $C_3H_9Si^+$ (73 *m/z*), and $C_3H_9OSi_2^+$ (117 *m/z*) and the negative ions CH_3SiO^- (59 *m/z*), SiO_2^- (60 *m/z*), and $CH_3SiO_2^-$ (75 *m/z*). Perfluorinated polyether residues are evidenced by the positive ions CFO^+ (47 *m/z*), $C_2H_3O_2^+$ (59 *m/z*), $C_2F_3O^+$ (97 *m/z*), $C_2F_4O^+$ (116 *m/z*), and $C_2F_5O^+$ (135 *m/z*) and the negative ions $C_2H_2FO^-$ (61 *m/z*) and $C_3H_3F_2O_2^-$ (109 *m/z*). In addition to process contaminants, common contaminants such as Na^+ (23 *m/z*), $^{39}K^+$ (39 *m/z*), $^{41}K^+$ (41 *m/z*) and adventitious hydrocarbons were observed in the positive ion spectra.

Upon α particle irradiation, changes in the signal of characteristic PTFE fragments were monitored, and new features in the mass spectra were identified and characterized. In most cases, emergent fragments appear in the mass spectra at intervals of 12, 16, 19, 31, and 50 *m/z* units corresponding to C, O, F, CF, and CF_2, respectively, whereby we are able to recognize families of related fragments. We have previously shown substantial evidence for the emergence and proliferation of hydrocarbons as well as oxyl- and peroxyl-functionalized fluorocarbon moieties.[7,8] For instance, evidence regarding the formation of peroxyl-functionalized fluorocarbons includes peaks at 125 *m/z* ($C_3F_3O_2^-$), 144 *m/z* ($C_3F_4O_2^-$), 137 *m/z* ($C_4F_3O_2^-$), and 156 *m/z* ($C_4F_4O_2^-$) in the negative ion spectra, as well as a similar succession of features in the positive ion spectra.

Reaction of α particle-generated fluorocarbon fragments to form hydroxyl-functionalized products is clearly indicated from the data. Evidence of such reactions is rendered in Figure 1 where the raw signals from the unirradiated and α-irradiated samples are presented. This figure shows the ions $C_4F_4H_2O^-$ and $C_4F_4H_2O_2^-$, at 142 and 158 *m/z*, respectively, to appear in the mass spectrum and increase in yield with increasing α dose. As demonstrated by these data, which are apparently void of isobaric interferences, the hydroxyl functionalities arise following α particle irradiation of the polymer matrix. These structures bear resemblance to the negative ions articulated in the preceding paragraph. The potential exists for at least two mechanisms that yield the same products. The first mechanism involves radiolytically induced reaction of fluorocarbon fragments with molecular oxygen followed by reaction with atomic or molecular hydrogen. The second mechanism involves radiolytically induced reaction of fluorocarbon fragments with molecular water and hydrogen peroxide, respectively. In each case, spontaneous (i.e., unimolecular) or induced (i.e., radiolytic) decomposition may participate in the mechanism. The mass windows presented in Figure 1 also reveal reaction between fluorocarbon fragments and silicone residues that are present in the PTFE matrix. The signals of $C_6F_9SiO^+$ (287 *m/z*) and $C_6F_9SiO_2^+$ (303 *m/z*), plotted as a function of α dose, are minimal at α doses $<10^9$ rad, after which the same signals become pronounced.

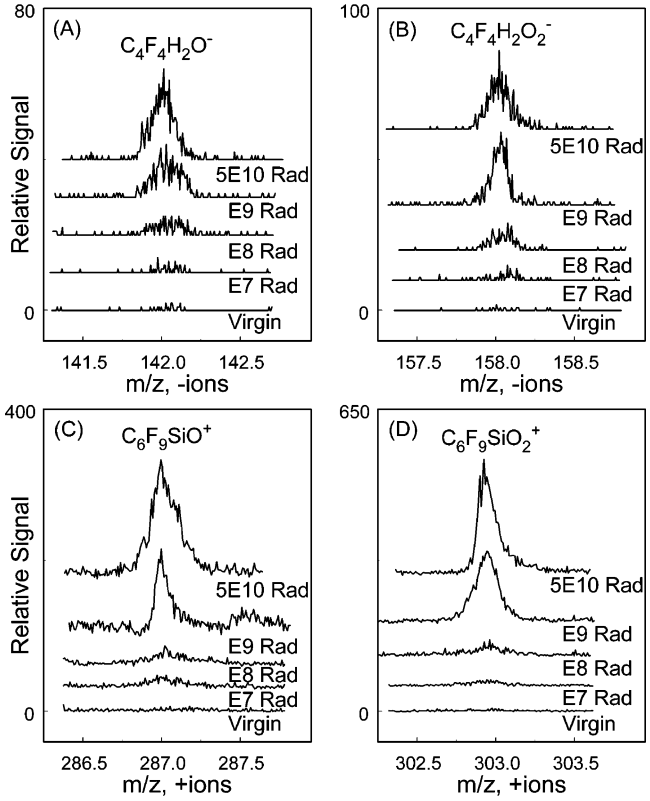

Figure 1. Unit mass windows demonstrating the appearance and ingrowth of hydroxyl- and silicate-functionalized fluorocarbon moieties with continued α particle irradiation of the PTFE matrix. Each plot includes the raw data at experimental doses of 0, 10^7, 10^8, 10^9, and 5×10^{10} rad. (A) Negative SIMS, 142 *m/z* nominal. (B) Negative SIMS, 158 *m/z* nominal. (C) Positive SIMS, 287 *m/z* nominal. (D) Positive SIMS, 303 *m/z* nominal. The offset is increased at higher doses for clarity.

The trends in the reaction of fluorocarbons to form hydroxyl-, peroxyl-, and silicate-functionalized moieties follow a reproducible pattern. Namely, considerable signals are realized at α doses $\geq 10^9$ rad, while the reactions seem to be moderated at α doses $\leq 10^8$ rad. Examples of the discontinuity that is manifested in the signals of fluorocarbon reaction products is given in the first four rows of Table 1 where, as is typical, a ~5-fold jump

TABLE 1: Tabulation of Data Discussed in the Text and Plotted in Figures 2 and 8

	virgin	10^7 rad	10^8 rad	10^9 rad	5×10^{10} rad
$C_3F_3O_2^+$	0	364	722	3472	9075
$C_4F_4H_2O_2^-$	0	84	93	577	2860
$C_6F_9SiO_2^+$	0	386	498	1619	4026
$C_3F_4O_2^-$	0	80	122	476	1467
CF_2O^+	897	2305	2540	7013	16071
H_2O^+	245	425	528	2272	7522
$C_3F_4O^+$	2977	4829	8185	16415	38823
$C_3F_7O^+$	2418	2629	3219	4812	10125
$C_2H_4^+$	3475	6918	9474	18447	29421
$C_2H_5^+$	18759	36655	46603	129032	186932
$C_2H_4O^+$	3408	4847	10336	16408	20912
$C_2H_4F^+$	0	2937	6687	8237	5448
$N_2H_4^+$	0	0	0	1548	2183

in the magnitude of the signals between 10^8 and 10^9 rad is clear. The CF_2O^+ fragment is an autolytic product of peroxyl fluorocarbon radicals.[16,17] These observations indicate that a threshold concentration of radicals must exist in the polymer matrix before a significant yield of the product is observed and allude to a diffusion-limited process that is in opposition to a mechanism dominated by surface reactions. In other words, reaction of α particle-generated fluorocarbon radicals with molecular gases incident at the sample surface cannot be the principle mechanism for the appearance of functionalized species in the mass spectra. A mechanism subject only to surface reactions would be expected to show an exponential relationship between α particle dose and reaction product yield. However, the data reveal a discontinuity in the signal at $\sim 10^9$ rad indicating that the reaction mechanism is initially constrained by the lack of free radical diffusion. Once free radical diffusion commences, the signals of the reaction products escalate as illustrated in Figure 2A−C. Therefore, while sources of oxygen are clearly present at the sample surface, sources of oxygen must also be located within the polymer matrix to explain the observed results.

Close inspection of the mass spectra reveals significant evidence to support the assertion that molecular gases are present in the PTFE matrix. Expanded portions of the mass spectra at 18, 28, 32, and 44 *m*/*z* are shown in Figure 3. Each plot includes the raw signals of the unirradiated and α-irradiated samples. The H_2O^+ ion appears at 18 *m*/*z*, accompanied by a small signal at 17 *m*/*z* corresponding to OH^+. At increasing levels of irradiation the signals of H_2O^+ and OH^+ reach significant intensities. The increasing signal of H_2O^+ with increasing α dose is an unexpected result that is consistent with the totality of the data, as will be explained later. Several isobaric species are observed at 28 *m*/*z* including Si^+, N_2^+, and $C_2H_4^+$. The signal of Si^+ remains relatively constant because it is a fragment ion of silicone residues that are dispersed throughout the polymer matrix. The materialization of N_2 and concurrent absence of CO within the polymer matrix is a significant observation that is in agreement with kinetic and thermodynamic data.[18−20] The presence of $C_2H_4^+$ in the unirradiated specimen is attributed to the presence of both adventitious hydrocarbons and isoparaffins,[9,10] while the subsequent increase in the signal of $C_2H_4^+$ is the result of isoparaffin radiolysis. The apparent rise in the N_2^+ peak is attributed to the overlapping $C_2H_4^+$ peak wherein, at high doses of α particles, the observed rise in the signal of $C_2H_4^+$ is accompanied by a slight broadening of the peak.

The positive ion of molecular oxygen (O_2^+) is recognized at 32 *m*/*z* along with isobaric peaks corresponding to CHF^+ and $N_2H_4^+$. The signal of O_2^+ remains relatively constant throughout the α irradiation regime while the emergence of both CHF^+ and $N_2H_4^+$ becomes pronounced at higher levels of α irradiation.

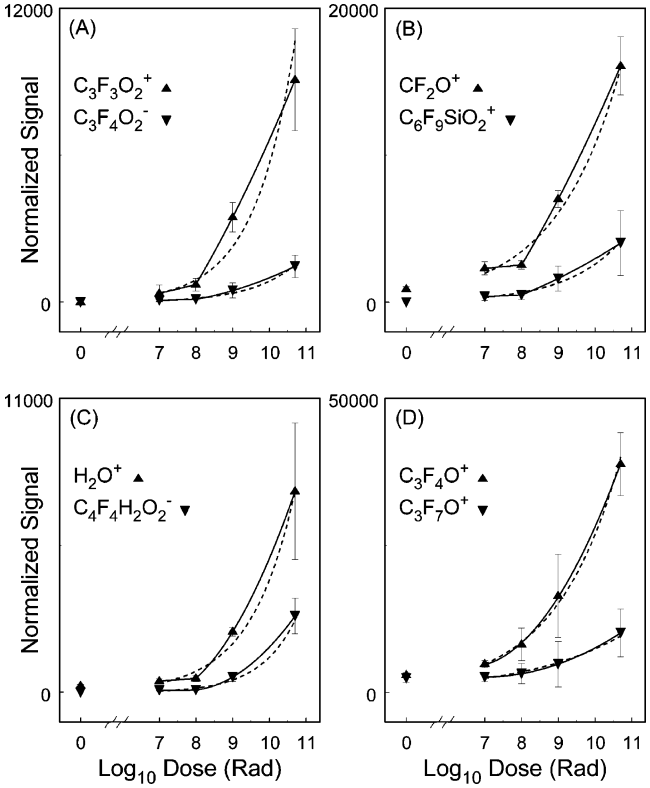

Figure 2. Integrated signals of radiolytic reaction products plotted vs the log of the dose. The data are normalized to the total ion signal and fit by functions described in the text. The solid lines (—) are comprised of linear and quadratic functions, and the dashed lines (- - -) are first-order exponential functions. The error bars indicate an interval of one standard deviation ($\pm 1\sigma$) from the mean. All data are disclosed in Table 1. The data points at 10^{10} rad are omitted because the signals of radiolytically induced reaction products, i.e., species arising in the irradiated portion of the sample, are suppressed at this α dose. This effect is documented in ref 8 and is presumed to be a consequence of surface roughness.

It should be noted that the $N_2H_4^+$ ion is the only reaction product involving N_2 that has been positively identified. Several isobaric species are observed at 44 *m*/*z* including SiO^+, CO_2^+, C_2HF^+, and $C_2H_4O^+$. The signal of SiO^+, while small, remains relatively constant because it is a fragment ion of silicone residues in the polymer matrix. The $C_2H_4O^+$ peak in the mass spectrum of the unirradiated specimen is likely an endgroup fragment of perfluorinated polyether. The signals of C_2HF^+ and $C_2H_4O^+$ intensify with increasing α dose as a result of radiolytically induced reaction. The signal of CO_2^+ is present in the unirradiated specimen and becomes diminished at the highest α dose. At first glance, the detection of CO_2^+ may be attributed to molecular carbon dioxide in the polymer matrix. However, the assignment of CO_2^+ as a product of radiolysis is qualified by other data. In fact, the changes observed in the signals of CHF^+, CO_2^+, C_2HF^+, and $C_2H_4O^+$ may be understood in terms of the free radical and polyene concentrations during α particle irradiation, as discussed in section 4. Nevertheless, the potential presence of molecular carbon dioxide cannot be dismissed based solely on these data.

Interpretation of the data presented in the preceding paragraphs is further clarified by the data in Figure 4. Unit mass windows at 34 and 45 *m*/*z* in the positive polarity, as well as 19 and 28 *m*/*z* in the negative polarity, are displayed. At 34 *m*/*z*, the appearance of $H_2O_2^+$ is realized at the lowest dose of α particles. The formation of H_2O_2 arises from α particle-induced interaction of the most abundant gases in the polymer

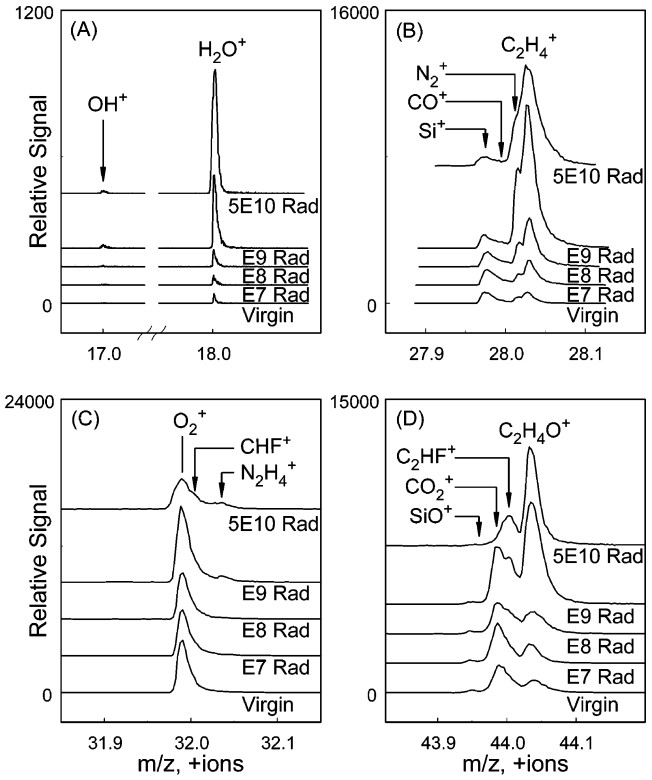

Figure 3. Expanded mass windows at nominal mass-to-charge ratios where molecular water, nitrogen, carbon monoxide, oxygen, and carbon dioxide appear in the mass spectra. Each plot includes the raw data at experimental doses of 0, 10^7, 10^8, 10^9, and 5×10^{10} rad. (A) Positive SIMS, 17 and 18 *m*/*z* centers. (B) Positive SIMS, 28 *m*/*z* nominal. (C) Positive SIMS, 32 *m*/*z* nominal. (D) Positive SIMS, 44 *m*/*z* nominal. The offset is increased at higher doses for clarity.

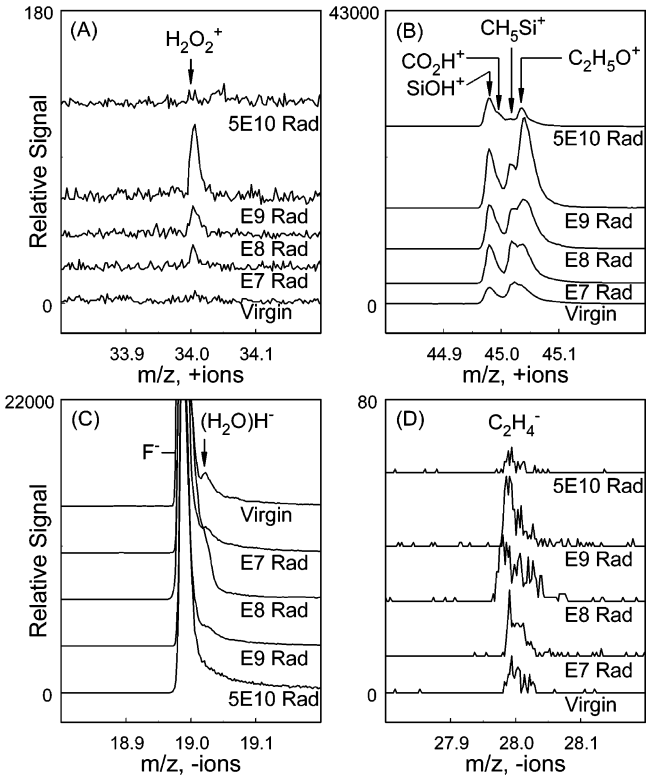

Figure 4. Unit mass windows supporting the data of Figure 3. Each plot includes the raw data at experimental doses of 0, 10^7, 10^8, 10^9, and 5×10^{10} rad. (A) Positive SIMS, 34 *m*/*z* nominal. (B) Positive SIMS, 45 *m*/*z* nominal. (C) Negative SIMS, 19 *m*/*z* nominal. (D) Negative SIMS, 28 *m*/*z* nominal. The scale of part C has been reduced by a magnitude of 5 to reveal the $(H_2O)H^-$ peak. The offset is increased at higher doses for clarity.

matrix, H_2 and O_2. Hydrogen peroxide is a comparatively unstable molecule which would presumably react to form hydroxylated moieties or decompose by spontaneous or induced means to H_2O and atomic O or an O• radical. These pathways are supported by the experimental data which confirm both the formation of hydroxyl-functionalized fluorocarbons (see Figure 1) and the profusion of H_2O (see Figure 3) with increasing α dose. The H_2O_2 peak vanishes from the spectrum at the highest α dose, an outcome that we propose is due to the burgeoning free radical and polyene concentrations.

The isobaric ions at 45 *m*/*z* include $SiOH^+$, CO_2H^+, CH_5Si^+, and $C_2H_5O^+$. The signals of both $SiOH^+$ and CH_5Si^+, which are fragment ions of silicone residues, remain relatively constant throughout the irradiation regime, though radiolytic decomposition results in a significant decline in the signal of CH_5Si^+ at the highest α dose. The signals of CO_2H^+ and $C_2H_5O^+$ that appear in the mass spectrum of the unirradiated specimen are likely protonated endgroup fragments of perfluorinated polyether. The intensity of the CO_2H^+ peak, while scarcely distinguishable as a shoulder on the $SiOH^+$ peak, remains relatively constant over the course of α irradiation. Again, the possibility that CO_2H^+ arises as a protonated ion of molecular carbon dioxide cannot be wholly dismissed based on these data. The signal of $C_2H_5O^+$ and of $C_2H_4O^+$ rises with increasing α particle irradiation and may be explained by both fragmentation of the perfluorinated polyether molecules and reaction of oxygen atoms, molecules, or radicals with hydrocarbon fragments. In contrast to the signal of $C_2H_4O^+$, the signal of $C_2H_5O^+$ diminishes at the highest α dose.

Confirmation of water in the polymer matrix is shown in the negative ion spectra which contain several peaks appearing at 19, 37, and 55 *m*/*z* that are recognized as clusters having the structure $(H_2O)_nX^-$ where X is a solvated H^- or F^- ion.[21] The portion of the mass spectra about 19 *m*/*z* in Figure 4C reveals a peak on the high-mass side of the F^- peak that is identified as $(H_2O)H^-$. The peaks at 37 and 55 *m*/*z*, not shown, correspond to the isobaric ions of $(H_2O)F^-$ and $(H_2O)_2H^-$, and $(H_2O)_2F^-$ and $(H_2O)_3H^-$, respectively. While the signal of H_2O^+ is observed to increase, the signals of the $(H_2O)_nX^-$ cluster ions wane at increasing levels of irradiation due to the declining localization of H^- and F^- anions (i.e., diffusion of H^- and F^- anions in the polymer matrix). The signal at 28 *m*/*z* in the negative polarity is comprised of $C_2H_4^-$ based on the rationale that molecular CO, which is more stable as a positive ion, is absent in the positive polarity.

We have previously used chemical imaging by TOF-SIMS to identify radiolytically induced reaction and decomposition products. Similarly, ion-specific images may be used to reinforce the veracity of claims derived from the mass spectral data concerning molecular gases. In particular, the signals of the intercalated molecular gases should not show a significant bias across the sample or with respect to α particle irradiation. Ion-specific images of N_2^+, O_2^+, CO_2^+, and $(H_2O)_nX^-$ are displayed in Figure 5; the total ion images of both the positive and negative polarities are provided as a reference to which topographically related artifacts may be compared. Some degradation of the signals of the total ion images is observed within the irradiated portion of samples and is attributed to surface roughening at high α doses. The image of $(H_2O)_nX^-$ is comprised of the isobaric $(H_2O)F^-$ and $(H_2O)_2H^-$ ions at 37 *m*/*z*. The ion-specific images of N_2^+, O_2^+, and $(H_2O)_nX^-$ illustrate that molecular nitrogen, oxygen, and water are uniformly distributed across

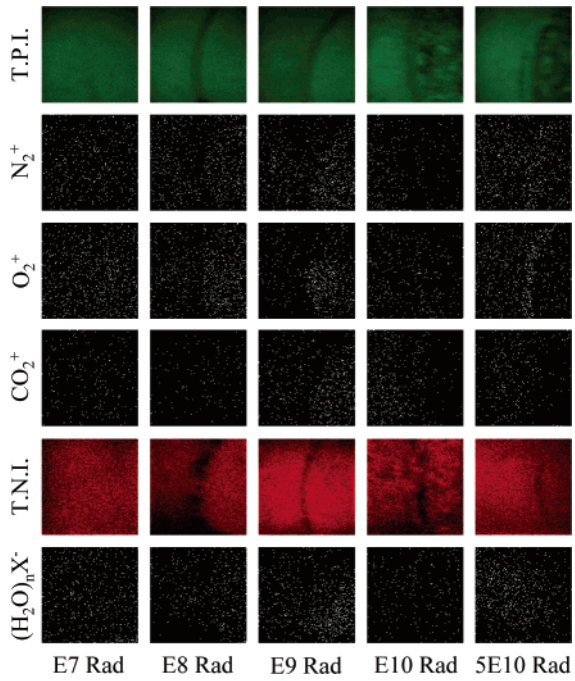

Figure 5. Positive and negative ion-specific images of α-irradiated PTFE at each experimental dose. Image sizes are 400 × 400 μm^2. Within each image, the irradiated portion of the sample is to the right while the unirradiated portion is to the left. The signals of emergent species are suppressed within the 10^{10} rad irradiation zone of all samples, although this effect is not obvious in these images since the imaged ions are not specifically a product of radiolysis. Images in each row are normalized to the same counts/pixel scale. Row 1: Total positive ion (T.P.I.) on a scale of 0−846. Row 2: N_2^+ on a scale of 0−1. Row 3: O_2^+ on a scale of 0−1. Row 4: CO_2^+ on a scale of 0−1. Row 5: Total negative ion (T.N.I.) on a scale of 0−62. Row 6: $(H_2O)F^-$ and $(H_2O)_2H^-$ on a scale of 0−1.

the sample and show no substantial bias with increasing α dose. The images of CO_2^+, in comparison to images of N_2^+ and O_2^+, show an increasingly diminished signal in the α-irradiated portion of the samples at 10^{10} and 5 × 10^{10} rad. This apparent disparity may be an indication that the signal of CO_2^+ arises from molecules that are subject to radiolytic decomposition, i.e., perfluorinated polyether. However, this interpretation is arguable, and the occurrence of CO_2 in the polymer matrix remains unsettled.

The RGA data, plotted in Figure 6, show the partial pressures of gas molecules liberated from PTFE during α particle irradiation. The samples were irradiated using a beam current of 40 nA which corresponds to a dose rate of 5 × 10^7 rad/s. The partial pressures of species at mass-to-charge ratios corresponding to H_2O^+ (18 *m*/*z*), CO^+/N_2^+ (28 *m*/*z*), O_2^+ (32 *m*/*z*), and CO_2^+ (44 *m*/*z*) were monitored concurrently during irradiation of the sample. Molecular hydrogen was not tracked during α particle irradiation of the sample because a reproducible baseline could not be established. The first indication of liberated gas molecules appears at 5 × 10^{10} rad where a distinct increase in the partial pressures of H_2O^+, CO^+/N_2^+, and O_2^+ are observed. Conspicuously absent from the RGA data is a rise in the partial pressure of CO_2. Therefore, the CO_2^+ and CO_2H^+ signals that arise in the TOF-SIMS data are definitively ascribed to perfluorinated polyether residues and radiolytic reaction products. Since the occurrence of CO gas is omitted based on the TOF-SIMS data, it is concluded that the observed rise in the 28 *m*/*z* trace of the RGA data is comprised almost completely of N_2 gas.

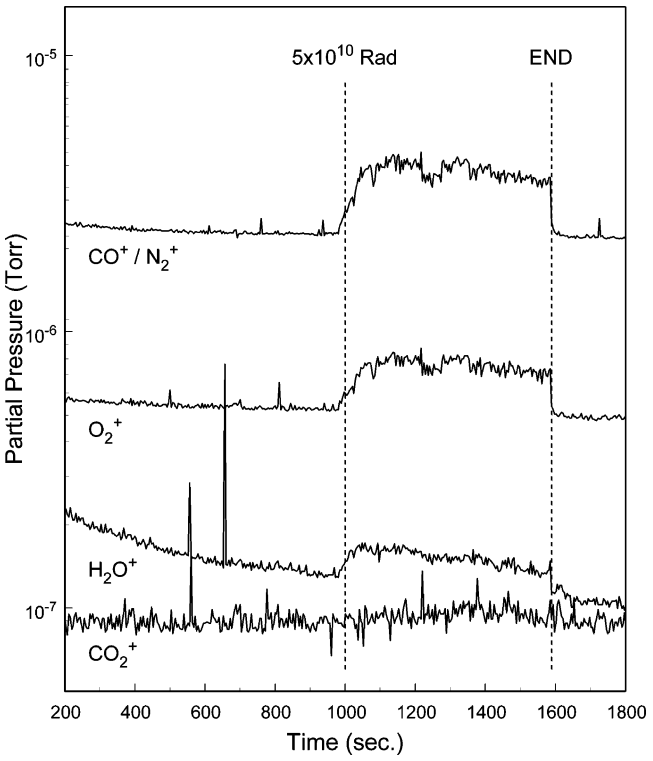

Figure 6. Residual gas analysis performed during α particle irradiation of PTFE. Traces are shown for H_2O^+ (18 *m*/*z*), CO^+/N_2^+ (28 *m*/*z*), O_2^+ (32 *m*/*z*), and CO_2^+ (44 *m*/*z*). The sample was irradiated at a rate of 5 × 10^7 rad/s. The first appearance of liberated gases is observed at ∼5 × 10^{10} rad; irradiation was terminated at 1580 s. As discussed in the text, the experimental evidence suggests that the rise in the 28 *m*/*z* trace is comprised of N_2 gas.

4. Discussion

The experimental data support the presence of N_2, O_2, and H_2O in the PTFE matrix. Moreover, H_2 is presumed to persist within the polymer matrix based on kinetic and thermodynamic[18−20] as well as TOF-SIMS[7] data. The occurrences of CO and CO_2 have been omitted based on the TOF-SIMS and RGA data, respectively. The relative abundances indicated by the data appear to lie in the descending order of H_2, O_2 > N_2 ≫ H_2O. Kinetic and thermodynamic data suggest that these observations are qualitatively correct. The permeability coefficients (*P*) and heats of solution (ΔH_s) for the detected molecular gases are H_2 > O_2 > N_2; no data are available regarding the permeability coefficient or heat of solution for H_2O. Pasternak et al. designate the magnitudes of the permeability coefficient and the heat of solution for CO_2 to be 3- and 2-times, respectively, the values obtained for O_2.[18] They also show that sorption and outgassing occur in a reversible fashion and that equilibrium is reached in a matter of minutes. Therefore, the absence of CO_2 gas in our experimental samples is explained by the low partial pressures to which the samples were exposed. Our experimental samples were stored in an ambient atmosphere (i.e., primarily N_2 and O_2), while irradiation and analysis was performed in a vacuum environment. The background of the vacuum environment during irradiation, as revealed in Figure 7, was comprised largely of H_2, H_2O, N_2, O_2, and CO_2 gases. Given the relatively low concentrations of CO_2 in the ambient and vacuum atmospheres to which the samples were exposed, it is reasonable to presume that little would be present in the experimental samples and observed in the data.

Radiolysis of H_2 leads to the proliferation of hydrocarbons and hydrogenated fluorocarbons as reaction products. Similarly,

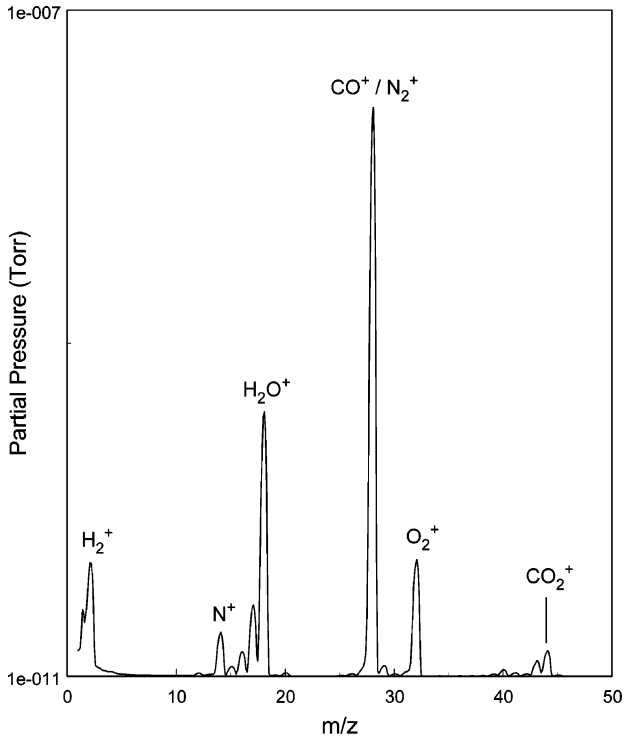

Figure 7. Gas background of the vacuum chamber obtained using a quadrupole-based RGA prior to α particle irradiation of the PTFE specimens.

radiolysis of O_2 leads to formation of oxyl- and peroxyl-functionalized hydrocarbons and fluorocarbons. Hydrogen and oxygen radicals interact to form H_2O_2, followed either by decomposition to water and atomic oxygen or by subsequent reaction to produce hydroxyl-functionalized species. Molecular nitrogen is also subject to radiolysis which is manifested in the formation of N_2H_4; however, there is no perceptible evidence to suggest that either N_2 or N_2H_4 participate in any further reactions. This seemingly enigmatic observation is understood to some extent by the bonding of the respective diatomic molecular gases present in the PTFE matrix. The dissociation energies of H−H, O═O, and N≡N are 436, 498, and 946 kJ/mol, respectively. We surmise that initial rupture of the π bonds in N_2 and O_2 molecules is partially negated by geminal recombination, on the time scale of a molecular oscillation ($\sim 10^{-13}$ s), before subsequent reactions may occur. Recombination of geminal radicals is known to occur in irradiated PTFE,[6,17,22] and in the case of N_2 there is a significant thermodynamic driver for recombination. At high doses of α particles, the concentration of H• radicals is such that reaction with N_2• radicals is readily observed. In other words, the thermodynamic barrier to rupture of the N≡N π bonds is not overcome but is kinetically driven by an excess of α particle-generated H• radicals. The spatial proximity of the H• and N_2• radicals is assumed to be small based on the rationale that the reaction must occur on the time scale of a molecular oscillation, the H_2 and N_2 gases are collocated within the polymer matrix,[18] and the samples are irradiated with a high LET source.[6] However, as indicated by the data for $N_2H_4^+$ in Table 1, this reaction is suppressed at low doses of α particles which presupposes the presence of radical scavengers. Without the presence of radical scavengers the signal of $N_2H_4^+$ would be expected to follow a simple exponential growth function.

In addition to α particle-induced reactions between intercalated molecular gases, we have noted that reactions leading to generation of functionalized fluorocarbons are moderated at doses $\leq 10^8$ rad. This observation is reflected in Figure 2 where the signals of $C_3F_3O_2^+$, $C_3F_4O_2^-$, $C_6F_9SiO_2^+$, $C_4F_4H_2O_2^-$, and H_2O^+, plotted as a function of α dose, all show a discontinuity between 10^8 and 10^9 rad. The data are fit by two relationships that are not representative of any particular model but demonstrate that the signals of certain reaction products do not display the anticipated exponential growth. The solid line is comprised of a linear function between 10^7 to 10^8 rad and a quadratic function between 10^8 and 5×10^{10} rad; the dashed line is a first-order exponential fit between 10^7 and 5×10^{10} rad. As shown by the data, only minimal growth of the signals is realized below 10^8 rad, while significant increases are realized above 10^8 rad. An exponential fit would be expected for reaction mechanisms unfettered by radical scavengers. In general, the exponential fits overestimate the signals at low dose and underestimate the signals at high dose. The signal of the CF_2O^+ ion, an autolytic decomposition product of peroxyl-functionalized fluorocarbon species,[16,17] follows the same trend, as expected. Noteworthy exceptions to this generalization are the signals of oxyl-functionalized fluorocarbon species, $C_3F_4O^+$ and $C_3F_7O^+$. These data exhibit no reproducible discontinuity between 10^8 and 10^9 rad and are fit quite well by both the quadratic and first-order exponential functions from 10^7 to 5×10^{10} rad. While oxyl-functionalized fluorocarbons are a product of α particle-induced reaction between fluorocarbon fragments and oxygen, these fragments also arise from radiolytic decomposition of perfluorinated polyether molecules that are present in the PTFE matrix. Radiolytic decomposition of perfluorinated polyether molecules would contribute to the observed oxyl signals most noticeably at low doses of α particles (i.e., $\leq 10^8$ rad).

We propose that, at low α doses, isoparaffins present in the PTFE matrix inhibit the radiation-induced reactions that give rise to emergent reaction products. Specifically, we surmise that hydrocarbon fragments arising from the radiolysis of isoparaffins behave as scavengers of H•, O•, and F• radicals; the radiolysis of aliphatic hydrocarbons results in production of polyenes and evolution of molecular hydrogen.[23−25] At α doses $\geq 10^9$ rad the inhibition appears to wane due to the burgeoning radical concentration that overwhelms the concentration of polyene scavengers in the polymer matrix. Evidence of such action is displayed in Figure 8 where the signals of $C_2H_4^+$, $C_2H_5^+$, $C_2H_4O^+$, and $C_2H_4F^+$ are plotted as a function of α dose. In Figure 8A the data are fit by two relationships for comparative purposes. The quadratic (solid line) and first-order exponential (dashed line) functions are fit to the data between 10^7 and 5×10^{10} rad. In Figure 8B the data are fit only by a quadratic function because an exponential growth model does not bear any resemblance to the trend of the data.

As shown in Figure 8, the signal of $C_2H_4^+$, which is representative of isoparaffin radiolysis (i.e., polyenes), rises at a modest rate with increasing α dose. Likewise, the signal of $C_2H_5^+$ intensifies with increasing α dose but at a higher rate. The initial signal of $C_2H_5^+$ is unquestionably characteristic of isoparaffin termini; however, the escalating signal of $C_2H_5^+$ and analogous fragments must be indicative of reaction between radiolized isoparaffins and H• radicals because radiolysis of aliphatic hydrocarbons results in unsaturation which would be evidenced by a decline in the signal of $C_2H_5^+$. This point is reinforced by the growing signal of $C_2H_4^+$ with increasing α dose. The signals of $C_2H_4O^+$ and $C_2H_4F^+$, which arise via reaction of radiolized isoparaffins with O• and F• radicals, respectively, rapidly swell upon irradiation of the PTFE specimens with α particles. These signals rise much more

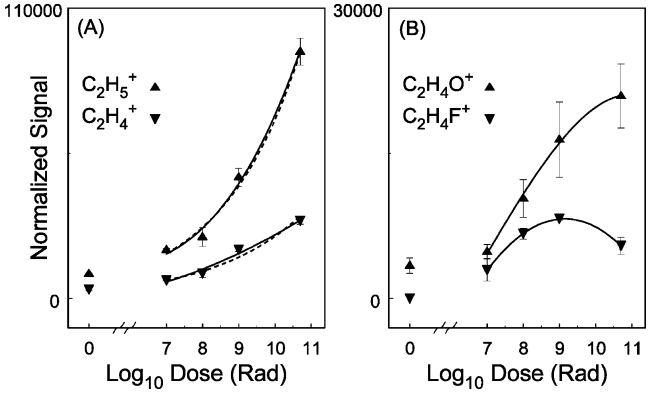

Figure 8. Integrated signals of radiolytic reaction products plotted vs the log of the dose. (A) Polyenes and hydrogenated polyenes are represented by the signals of $C_2H_4^+$ and $C_2H_5^+$, respectively. (B) Fluorinated and oxygenated polyenes are represented by the signals of $C_2H_4F^+$ and $C_2H_4O^+$, respectively. The data are normalized to the total ion signal and fit by functions described in the text. The solid lines (—) are comprised of linear and quadratic functions, and the dashed lines (- - -) are first-order exponential functions. The signal of $C_2H_5^+$ is divided by two. The error bars indicate an interval of one standard deviation ($\pm 1\sigma$) from the mean. All data are disclosed in Table 1. The data points at 10^{10} rad are omitted because the signals of radiolytically induced reaction products, i.e., species arising in the irradiated portion of the sample, are suppressed at this α dose. This effect is documented in ref 8 and is presumed to be a consequence of surface roughness.

rapidly than can be accounted for by radiolytic decomposition of perfluorinated polyether molecules. The signals of both $C_2H_4O^+$ and $C_2H_4F^+$ show a reduction in the rate of rise, or even a decline, at α doses $>10^9$ rad. The decline observed in the signal of $C_2H_4O^+$ and of $C_2H_4F^+$ is explained by gross radiolytic decomposition of the PTFE matrix at high doses of α particles[7] that facilitates small molecule and radical diffusion. The signal of $C_2H_5^+$ continues to enlarge at high α doses which is explained by reaction of isoparaffin unsaturations with H· radicals from both radiolyzed isoparaffins and intercalated H_2. This supposition is supported by a concomitant depression in the $C_2H_4^+$ signal at high doses of α particles (i.e., $>10^9$ rad).

Thus, our data indicate that incident MeV α particles commence a complex reaction process involving PTFE matrix molecules, manufacturing residues, intercalated molecular gases, and a plethora of α particle-generated radicals. The major features of the data are represented in Figure 9 by a simplified set of kinetic expressions that capture the observed reactants and functionalized fluorocarbon products. Reactions involving polyenes from radiolized isoparaffins are omitted because the radical scavenging of unsaturated hydrocarbons has been discussed elsewhere.[23−25] We note at the outset that these expressions do not likely capture all possible kinetic pathways but are proposed as a means to address our data and engender discussion. Equation 1A indicates the initial cleavage of C−F bonds in the fluoropolymer resulting in fluorocarbon and F· radicals. For brevity in the text, fluorocarbon fragments and radicals will be generically referred to as FC and FC·, respectively. The F· radicals may then react with C−C bonds of the polymer to generate a saturated chain end and a terminal double bond, as expressed by eq 1B. Main chain scission, i.e., C−C bond cleavage by incident α particles, is shown in eq 1C. Many articles, wherein low LET sources are used to irradiate the PTFE samples, neglect main chain scission on the basis that caging results almost exclusively in reconstitution of the C−C bonds;[17,22] however, our data indicate that irradiation of the PTFE samples with α particles, a high LET source, results in a

1A. $-(CF_2)_n- + \alpha \leftrightarrow -(CF_2)_x-CF\cdot-(CF_2)_y- + F\cdot$
1B. $F\cdot + -(CF_2)_n- \leftrightarrow -(CF_2)_x-CF{=}CF_2 + CF_3-(CF_2)_y- + F\cdot$
1C. $-(CF_2)_n- + \alpha \leftrightarrow -(CF_2)_x\cdot + \cdot(CF_2)_y-$

2A. $H_2 + O_2 + \alpha \leftrightarrow H_2O_2$
2B. $2H\cdot + O_2 + \leftrightarrow H_2O_2$
2C. $H_2 + 2O\cdot + \leftrightarrow H_2O_2$
2D. $O\cdot + H_2O \leftrightarrow H_2O_2\cdot \;//\; O + H_2O\cdot \leftrightarrow H_2O_2\cdot$

3A. $F\cdot + H_2 \leftrightarrow HF + H\cdot$
3B. $FC\cdot + xH_2 \leftrightarrow FCH_{2x-1} + H\cdot$

4A. $FC\cdot + O_2 \leftrightarrow FCO_2\cdot \leftrightarrow F_{x-1}CO_2 + F\cdot$
4B. $FCO_2\cdot \leftrightarrow FCO\cdot + O \leftrightarrow F_{x-1}CO + O + F\cdot$
4C. $FCO_2\cdot \leftrightarrow FCO\cdot + CF_2O \leftrightarrow F_{x-1}CO + F\cdot$
4D. $FC\cdot + O \leftrightarrow FCO\cdot \leftrightarrow F_{x-1}CO + F\cdot$

5A. $FC + H_2O_2 \leftrightarrow FC(OH)_2$
5B. $FCO\cdot + H_2O \leftrightarrow FC(OH)_2\cdot \leftrightarrow F_{x-1}C(OH)_2 + F\cdot$
5C. $FC\cdot + H_2O \leftrightarrow FCH_2O\cdot \leftrightarrow F_{x-1}CH_2O + F\cdot$
5D. $FC\cdot + H_2O \leftrightarrow FCH_2O\cdot \leftrightarrow FCOH + H\cdot$
5E. $FCO_2\cdot + H_2 \leftrightarrow FC(OH)_2\cdot \leftrightarrow F_{x-1}C(OH)_2 + F\cdot$
5F. $FCO\cdot + H_2 \leftrightarrow FCH_2O\cdot \leftrightarrow F_{x-1}CH_2O + F\cdot$
5G. $FCO\cdot + H_2 \leftrightarrow FCH_2O\cdot \leftrightarrow FCOH + H\cdot$

Figure 9. Set of kinetic expressions that capture the reactants and functionalized fluorocarbon products observed in the experimental data. References to previous work are given and discussed in the text. Fluorocarbon fragments such as $-(CF_2)_n-$ or C_nF_m are generically denoted by "FC" in the equations except in eq 5A where "FC" represents a perfluoroalkene having the structure $-(CF_2)_x-CF{=}CF-(CF_2)_y-$ or $-(CF_2)_x-CF{=}CF_2$. Reactions involving N_2 are omitted since no nitrogen-functionalized fluorocarbon products are observed in the data.

demonstrable change in the chemical structure that is attributable to main chain scission.[7]

Equations 2A−D describe a most interesting consequence of α radiolysis discovered in our data. Namely, the α particle-initiated reaction between H_2 and O_2 to yield H_2O_2 is quite pronounced. There are several reactions that potentially generate H· or O· radicals as secondary products that would be available for further reaction to yield H_2O_2, as indicated in eqs 2B and 2C. Additionally, H_2O may participate in the production of H_2O_2 as indicated in eq 2D; however, this mechanism is presumed to be of little consequence based on the low initial abundance of H_2O and strong evidence that H_2O_2 decomposes to H_2O and O. In other words, the decomposition of H_2O_2 drives the reaction in eq 2D toward the reactants.

The eqs 3A and 3B show reaction of the FC· and F· radicals with molecular H_2 yielding H· radicals, HF, and FCH_{2x-1}. Many fragment ions in the mass spectra confirm the production of FCH_{2x-1} species, as illustrated in Figure 3. Hydrogen fluoride (HF) is shown by our data to be a product of insignificant yield. Moreover, polyene hydrocarbon fragments and F· radicals are shown to interact to produce $C_xH_yF_z^{\pm}$ moieties. Equations 4A−D show the reaction of FC· radicals with molecular O_2 yielding oxyl- and peroxyl-functionalized fluorocarbons. Both oxyl and peroxyl species are observed in the mass spectra, and their radicals are presumed to terminate, or neutralize, via the release of F· radicals.[17,22] We suspect that ejected F· radicals largely stimulate further back-biting reactions, as in eq 1B. This conjecture is based on the signals of both F^- and F_2^- that decline as a function of α dose and the signals of small fluorocarbon fragments that escalate as a function of α dose. Several studies have implicated a second-order mechanism for the production of oxyl species,[3,8,16,17,25] and we postulate the pathways shown in eqs 4B−D to address these data. The mechanism of eq 4B is validated by previous work,[3,17] while the mechanism of eq 4D is facilitated by both the radiolysis of molecular oxygen and

the decomposition of H_2O_2. Equation 4C is confirmed by our observation of CF_2O which is a verified decomposition product of peroxyl-functionalized fluorocarbon radicals.[16,17,25] Generation of atomic oxygen is supported by our data which show an increase in the signal of O^- with increasing α dose.

The products or intermediates of the aforesaid expressions may participate in further reactions, noted in eqs 5A−G, to produce the hydroxyl-functionalized fluorocarbons that are observed in the experimental data. We propose that the most favorable reaction mechanisms involve the reaction of fluorocarbon (FC•), oxyl (FCO•), or peroxyl (FCO_2•) radicals with H_2O or H_2 to produce the observed hydroxylated moieties. The reaction of perfluoroalkenes, such as $-(CF_2)_x-CF{=}CF-(CF_2)_y-$ and $-(CF_2)_x-CF{=}CF_2$, with H_2O_2 to yield hydroxylated moieties (eq 5A) seems reasonable based on the data. In each case, further rearrangement of bonds within the intermediates to form a more thermodynamically stable entity, accompanied by the loss of H• or F• radicals, is presumed to occur. We see no evidence in the TOF-SIMS data to suggest that significant quantities of $\sim(CF_2)_xCO_2H$ are produced. We conclude that the $-CO_2H$ groups observed in our data are the result of interactions between hydrocarbon polyenes and molecular oxygen.

A great deal of work remains concerning the mechanisms and kinetics of reactions that are precipitated by α particle irradiation of PTFE. Specifically, none of the rate constants have been evaluated for even the most basic effects of α radiolysis in PTFE, e.g., C−C scission, C−F scission, and back-biting reactions. There are several factors that have a deleterious effect on the quantification of the experimental data. First, each decade increase in the dose of α particles incident on the sample has a demonstrable impact on the surface topography, as illustrated in Figure 5. It is expected that a corresponding change in the surface work function (Φ_s) would be realized; however, we have not executed measurements against which to normalize our experimental data. Rather, we have normalized our data against either a reference ion signal or the total ion signal. Second, ionization efficiencies may change dramatically from ion to ion. Therefore, while relative quantification is feasible, absolute quantification is difficult without a reference, or corroborating data. Third, the microscopic structure of PTFE is comprised of crystalline and amorphous regions. Therefore, the products of α radiolysis are not homogeneously distributed. We have attempted to minimize this effect by sampling large areas of the surface. Fourth, radiolysis is a dynamic process wherein fragmentation and defluorination occur concurrently with other α particle-induced reactions. Consequently, difficulties in the quantification of functionalized fluorocarbon moieties are exacerbated by the fragmentation and defluorination of analyte fragments with increasing α dose. This competition is most pronounced for high-mass fragment ions wherein the fluorine content is saturated but is also observed in relatively small fragments. The latter remark is demonstrated in the plots of the $C_3F_4O^+$ and $C_3F_7O^+$ signals as a function of α dose in Figure 2D. The signal of the more fully saturated fragment ($C_3F_7O^+$) does not rise as rapidly as that of the more unsaturated fragment ($C_3F_4O^+$). These circumstances, which contribute to a comparatively large statistical fluctuation in the experimental data, might be mitigated in future experiments with the use of additional chemical and structural probes such as XPS, IRS, and differential scanning calorimetry (DSC). Even so, the effects of α particle radiolysis observed in our data are reproducible and bear resemblance to previous work in which unsaturated hydrocarbons were shown to have the effect of radiation protection via radical scavenging.[23−25]

Future experiments may be conducted so as to isolate the reactions between fluorocarbon radicals and gases of interest. Experiments of this type require thorough degassing of the experimental samples followed by exposure to high-purity gases prior to α particle irradiation. The long lifetimes of fluorocarbon radicals within the polymer matrix would necessitate storage of the experimental samples under the same atmosphere in which irradiation was performed.[22] Such an experimental scheme would allow the elucidation of the relative rates of reaction between specific molecular gases and radiolytically generated fluorocarbon radicals. For example, use of isotopically labeled $^{18}O_2$ would allow one to resolve whether unimolecular decomposition of dioxide fragments is the primary mechanism giving rise to monoxide fragments. Furthermore, the use of isotopically labeled oxygen would allow interrogation of the process that gives rise to copious quantities of H_2O in the polymer matrix. We have shown the presence of molecular CO_2 in our experimental specimens to be negligible. Nevertheless, the inclusion of isotopically labeled $^{13}CO_2$ would enable the differentiation of α particle-induced reaction products from perflourinated polyether fragments in the mass spectra which would serve as a test against which to verify our conclusions. Continued investigation seems particularly important in light of the fact that PTFE has been shown to be permeable to N_2, which is observed in both the TOF-SIMS and RGA data, yet no nitrogen-functionalized fluorocarbon species are identified in the TOF-SIMS spectra of the α-irradiated specimens. To execute these experiments, a new chamber for attachment to the tandem accelerator beam line has been designed with a vastly reduced volume that will also allow positioning of the RGA within 1 in. of the sample. The chamber is isolated from the beam line by a 20 μm thick Havar (Co−Cr−Ni alloy) foil which will allow exposure of the PTFE samples to various gases at atmospheric pressure without affecting the performance of the beam line.

5. Conclusions

Our data indicate that MeV α particles incident on PTFE beget a complex reaction process involving PTFE matrix molecules, manufacturing residues, and intercalated molecular gases. Molecular gases identified in the polymer matrix are H_2, H_2O, N_2, and O_2; the data show no evidence to suggest the presence of CO and CO_2 in the polymer matrix. In addition to previous data[7,8] regarding the emergence of hydro-, oxyl-, and peroxyl-functionalized fluorocarbons, we have disclosed evidence demonstrating the production of hydroxyl-functionalized fluorocarbons by way of α particle-initiated reactions between fluorocarbon fragments and molecular gases. We have proposed a set of kinetic expressions that address the prominent features observed in our data without contradicting previously validated reaction mechanisms.[16−18,22−25] Without question, these mechanisms neglect the intermediate, dynamic processes since we are only able to identify the stable products of reaction and decomposition. Nevertheless, the proposed kinetic expressions provide a basis from which to interrogate systematically the α radiolysis of PTFE in ambient and vacuum atmospheres. We have also provided evidence to suggest that the kinetics of α particle-induced reactions in PTFE are initially suppressed by small hydrocarbon fragments. These hydrocarbon fragments, which arise from radiolytic decomposition of isoparaffins in the polymer matrix, are shown to be scavengers of H•, O•, and F• radicals and, thereby, limit the rates of reaction. Above a

threshold dose of α particles, the concentration of radicals exceeds that of the scavengers and free radical diffusion commences resulting in an increased yield of reaction products. While the radiation stabilization afforded by the presence of isoparaffins is indeed feeble, the effect is self-evident. The threshold dose in our experiments was $\sim 10^8$ rad; however, the threshold dose should be dependent on the concentration of isoparaffins in the polymer matrix. This theory may easily be tested by varying the concentration of isoparaffins in the PTFE matrix.

Acknowledgment. G.L. Fisher would like to acknowledge the assistance of Chad Meserole in critical discussions and review of this manuscript. Financial support for this research was provided by the United States Department of Energy under Contract No. W-7405-ENG.

References and Notes

(1) Fischer, D.; Lappan, U.; Hopfe, I.; Eichhorn, K. J.; Lunkwitz, K. *Polymer* **1998**, *39*, 573.

(2) Lappan, U.; Geissler, U.; Haussler, L.; Jehnichen, D.; Pompe, G.; Lunkwitz, K. *Nucl. Instrum. Methods Phys. Res., Sect. B* **2001**, *185*, 178.

(3) Burger, W.; Lunkwitz, K.; Pompe, G.; Petr, A.; Jehnichen, D. *J. Appl. Polym. Sci.* **1993**, *48*, 1973.

(4) Wilson, D. J.; Williams, R. L.; Pond, R. C. *Surf. Interface Anal.* **2001**, *31*, 385.

(5) Heitz, J.; Niino, H.; Yabe, A. *Jpn. J. Appl. Phys.* **1996**, *35*, 4110.

(6) Lee, E. H. *Nucl. Instrum. Methods Phys. Res., Sect. B* **1999**, *151*, 29.

(7) Fisher, G. L.; Ohlhausen, J. A.; Wetteland, C. J. *Surf. Interface Anal.* **2005**, *37*, 713.

(8) Fisher, G. L.; Szakal, C.; Wetteland, C. J.; Winograd, N. Article to appear in the AVS 52nd International Symposium Proceedings, *J. Vac. Sci. Technol. A*, Jul/Aug 2006.

(9) Ariawan, A. B.; Ebnesajjad, S.; Hatzikiriakos, S. G. *Powder Technol.* **2001**, *121*, 249.

(10) Ariawan, A. B.; Ebnesajjad, S.; Hatzikiriakos, S. G. *Polym. Eng. Sci.* **2002**, *42*, 1247.

(11) Braun, R. M.; Blenkinsopp, P.; Mullock, S. J.; Corlett, C.; Willey, K. F.; Vickerman, J. C.; Winograd, N. *Rapid Commun. Mass Spectrom.* **1998**, *12*, 1246.

(12) Weibel, D.; Wong, S.; Lockyer, N.; Blenkinsopp, P.; Hill, R.; Vickerman, J. C. *Anal. Chem.* **2003**, *75*, 1754.

(13) Briggs, D. *Surf. Interface Anal.* **1990**, *15*, 734.

(14) Newman, J. G.; Carlson, B. A.; Michael, R. S.; Moulder, J. F. *Static SIMS Handbook of Polymer Analysis*; Physical Electronics: Eden Prairie, MN, 1991.

(15) Briggs, D. *Surf. Interface Anal.* **1989**, *14*, 209.

(16) Matveev, V. K.; Klinshpont, E. R.; Surnin, V. A.; Kiryukhin, V. P.; Milinchuk, V. K. *Polym. Sci. U.S.S.R.* **1990**, *32*, 593.

(17) Gross, U.; Dietrich, P.; Engler, G.; Prescher, D.; Schulze, J.; Lunkwitz, K.; Ferse, A. *J. Fluorine Chem.* **1982**, *20*, 33.

(18) Pasternak, R. A.; Christensen, M. V.; Heller, J. *Macromolecules* **1970**, *3*, 366.

(19) Brandt, W. W.; Anysas, G. A. *J. Appl. Polym. Sci.* **1963**, *7*, 1919.

(20) Michaels, A. S.; Bixler, H. J. *J. Polym. Sci.* **1961**, *L*, 393.

(21) Wojciechowski, I. A.; Kutliev, U.; Sun, S.; Szakal, C. W.; Winograd, N.; Garrison, B. J. *Appl. Surf. Sci.* **2004**, *231*−*232*, 72.

(22) Forsythe, J. S.; Hill, D. J. T. *Prog. Polym. Sci.* **2000**, *25*, 101.

(23) Fallgatter, M. B.; Dole, M. *J. Phys. Chem.* **1964**, *68*, 1988.

(24) Soebianto, Y. S.; Katsumura, Y.; Ishigure, K.; Kubo, J.; Koizumi, T.; Shigekuni, H.; Azami, K. *Polym. Degrad. Stab.* **1993**, *42*, 29.

(25) Milinchuk, V. K. *Nucl. Instrum. Methods Phys. Res., Sect. B* **1995**, *105*, 24.